

New Heteroleptic Germanium Precursors for GeO₂ Thin Films by Atomic Layer Deposition

Heenang Choi, Chanwoo Park, Sung Kwang Lee, Ji Yeon Ryu, Seung Uk Son, Taeyong Eom,* and Taek-Mo Chung*



Cite This: *ACS Omega* 2023, 8, 43759–43770



Read Online

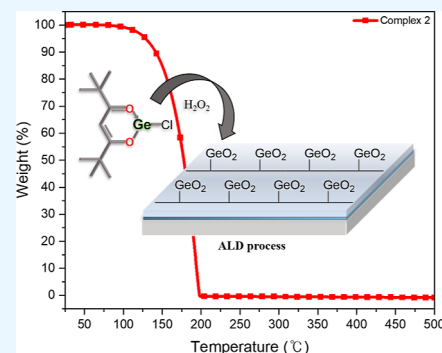
ACCESS |

Metrics & More

Article Recommendations

Supporting Information

ABSTRACT: This study describes the synthesis of 12 new germanium complexes containing β -diketonate and/or *N*-alkoxy carboxamidate-type ligands as precursors for GeO₂ through atomic layer deposition (ALD). A series of Ge(β -diketonate)Cl complexes such as Ge(acac)Cl (**1**) and Ge(tmhd)Cl (**2**) were synthesized by using acetylacetonate (acacH) and 2,2,6,6-tetramethyl-3,5-heptanedione (tmhdH). *N*-Alkoxy carboxamidate-type ligands such as *N*-methoxypropanamide (mpaH), *N*-methoxy-2,2-dimethylpropanamide (mdpaH), *N*-ethoxy-2-methylpropanamide (empaH), *N*-ethoxy-2,2-dimethylpropanamide (edpaH), and *N*-methoxybenzamide (mbaH) were used to afford further substituted complexes Ge(acac)(mpa) (**3**), Ge(acac)(mdpa) (**4**), Ge(acac)(empa) (**5**), Ge(acac)(edpa) (**6**), Ge(acac)(mba) (**7**), Ge(tmhd)(mpa) (**8**), Ge(tmhd)(mdpa) (**9**), Ge(tmhd)(empa) (**10**), Ge(tmhd)(edpa) (**11**), and Ge(tmhd)(mba) (**12**), respectively. Thermogravimetric analysis curves, which mostly exhibited single-step weight losses, were used to determine the evaporation properties of complexes **1**–**12**. Interestingly, liquid complex **2** has no residue at 198 °C and therefore exhibits excellent vaporization properties and high volatility. Single-crystal X-ray diffraction studies of **1** and **7** demonstrated that the complexes had monomeric molecular structures with germanium chelated by the oxygen atoms of one or two bidentate ligands, respectively. An ALD process was developed for the growth of GeO₂ using Ge(tmhd)Cl (**2**) as a new precursor and H₂O₂ as an oxidant. This study demonstrates the achievement of self-limiting growth of GeO₂ films by varying the duration of injection/purge, with an observed ALD window at deposition temperatures ranging from 300 to 350 °C. The saturated growth per cycle of the GeO₂ film was determined as 0.27 Å/cycle at a deposition temperature of 300 °C. The deposited films were observed to be amorphous consisting of GeO₂.



INTRODUCTION

Oxides of group 14 have been used in various technical applications such as semiconductors, sensors, and catalysts. Among these, silicon dioxide is commonly used during the manufacture of electronic products, whereas tin dioxide, for instance, is used in transparent conductive oxides and gas sensors.^{1–7} Germanium-based oxides, which are relatively less researched than other oxides, have several phases, such as GeO, Ge₂O, GeO₂, and Ge₂O₃.⁸ These types of germanium oxide were attractive materials such as both amorphous-form GeO_x and crystalline-form GeO₂ owing to their optical and electrical properties. GeO₂ is used as a high- κ interlayer dielectric material and is useful in high-frequency applications because of its high carrier mobility.^{9–11} In particular, GeO₂ can be used as a blocking layer with a reasonable band gap (5.81 eV) and a higher dielectric constant ($\kappa \approx 6$) than SiO₂ ($\kappa \approx 3.9$).^{12,13} In addition, GeO₂ is commonly used in various applications such as electro-optical modulators, fiber optic materials,^{14,15} nonlinear optics,^{16,17} and piezoelectric glass materials¹⁸ and can be applied in batteries for rapid charging or discharging in lithium or sodium batteries.^{19–25} GeO₂ nanoparticles can be used as memory devices or photocatalysts,

and previous research has demonstrated the typical properties of the charge-storage effect of GeO₂ nanoparticles.^{26–28} Amorphous GeO₂ is a good glass former and competitive with α -SiO₂ or amorphous boron oxide.^{29,30} Furthermore, germanium is an attractive substitute for SiO₂ in metal-oxide-semiconductor field-effect transistors.^{31–35} Germanium oxide-based electronic devices are of interest to researchers because of their broad range of applications. Additionally, hexagonal GeO₂ and amorphous GeO₂ possess water solubility, prompting research into their potential utilization in emerging applications such as secure elements and eco-friendly processes.^{8,36,37} Consequently, the development of germanium oxides with tuned defects, vacancies, and high stoichiometries is necessary to increase their potential for various applications. Widely used thin-film processes include sputtering, thermal

Received: August 2, 2023

Revised: October 13, 2023

Accepted: October 18, 2023

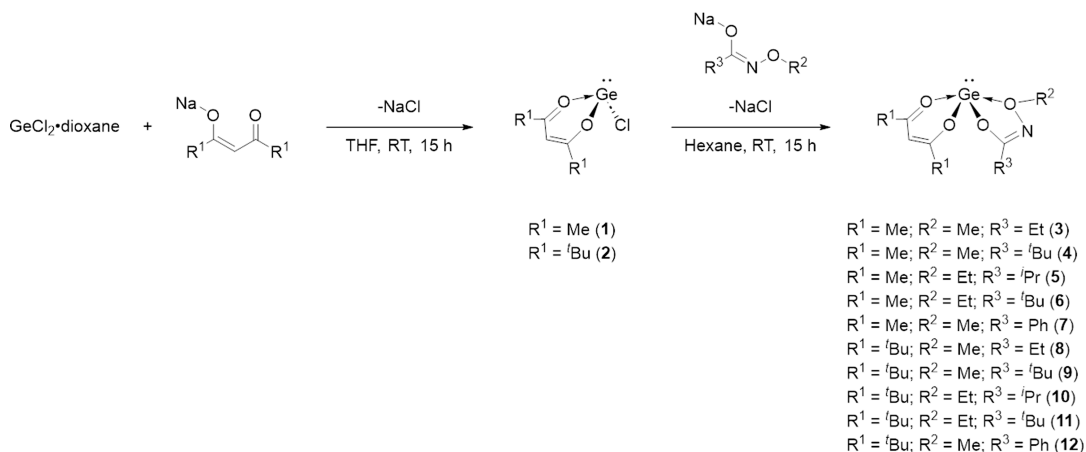
Published: November 9, 2023



Table 1. Summary of the ALD Process of the GeO₂ Film

| precursor | oxidant | GPC (Å/cycle) | ALD window (°C) | reference |
|---|----------------|---------------|-----------------|-----------|
| Ge(dpp-BIAN) | O ₃ | 0.5 | N/A | 13 |
| Ge(NMe ₂) ₂ (NH ^t Pr(CH ₂) ₂ NH ^t Pr) | O ₃ | 0.4 | 200–320 | 50 |
| Ge(NMe ₂) ₂ (NH ^t Bu(CH ₂) ₂ NH ^t Bu) | O ₃ | 0.31 | 200–320 | 50 |
| Ge(NMe ₂) ₄ | O ₃ | 0.45 | 180–230 | 8 |
| Ge(O ^t Bu) ₄ | O ₃ | 0.3 | 200–330 | 8 |

Scheme 1. Synthesis of the Germanium Complexes 1–12



processing, and chemical vapor deposition (CVD).^{38–45} However, these methods have drawbacks such as low conformality, poor thickness controllability, and uniformity, and most of the Ge oxides produced in these processes exhibit mixed chemical composition rather than a single-composition material. In contrast, atomic layer deposition (ALD), which is advantageous for nanosized device manufacturing, forms highly stoichiometric GeO₂ films with properties such as atomic-scale thickness control, excellent conformality, and low impurity contamination.^{33,46–51} Ge(NMe₂)₄, Ge(O^tBu)₄,⁸ Ge(dpp-BIAN) (1,2-bis[(2,6-diisopropylphenyl)imino]acenaphthene: dpp-BIAN),¹³ Ge(NMe₂)₂(NH^tPr(CH₂)₂NH^tPr), and Ge(NMe₂)₂(NH^tBu(CH₂)₂NH^tBu)⁵² have been reported as germanium precursors for the ALD process. However, it is often difficult for homoleptic complexes to adopt the desired reactivity and stability by the uniformity of the ligands, whereas heteroleptic compounds with two or more types of different ligands might give interesting alternatives such as high volatility, stability, and desired reactivity relatively compared to homoleptic complexes.⁵³ Additionally, Ge oxide is still relatively unexplored compared to SiO₂ in thin-film processes using ALD technology; further research is required. Table 1 presents a comprehensive overview of various investigations focused on the ALD-based GeO₂ deposition method.⁵⁴ Notably, the reported studies exclusively examined the deposition, employing O₃ as a reactant. Additionally, given the requirement to modify the properties of the thin film, it has become essential to perform depositions at higher temperatures than previously employed. Consequently, there is a clear need to develop a novel GeO₂ ALD process utilizing an alternative precursor that will broaden the spectrum of available oxidants and process temperatures, thereby enhancing the versatility of the deposition technique.

In this study, we newly synthesized germanium precursors for germanium oxide thin films. By demonstrating capability using the ALD process, the synthesized new germanium

complexes have the possibility to promote in-depth research in various fields where germanium oxide is used. To synthesize new germanium precursors, we extended our previous study of homoleptic divalent germanium and tin compounds containing *N*-alkoxy carboxamide ligands.⁵⁵ Complexes using β -diketonate ligands have generally been widely used for precursors.^{56–58} To the best of our knowledge, the β -diketonate ligand system has not been explored in the field of Ge precursors as a heteroleptic complex using carboxamide ligands. Therefore, we used β -diketonate ligands, namely, acac (acetylacetonate) and tmhd (2,2,6,6-tetramethyl-3,5-heptanedioate), and prepared a series of *N*-alkoxy carboxamide, namely, *N*-methoxypropanamide (mpaH), *N*-methoxy-2,2-dimethylpropanamide (mdpaH), *N*-ethoxy-2-methylpropanamide (empaH), *N*-ethoxy-2,2-dimethylpropanamide (edpaH), and *N*-methoxybenzamide (mbaH), along with the corresponding germanium complexes. We synthesized complexes Ge(acac)Cl (1) and Ge(tmhd)Cl (2), and obtained the heteroleptic compounds Ge(acac)(mpa) (3), Ge(acac)(mdpa) (4), Ge(acac)(empa) (5), Ge(acac)(edpa) (6), Ge(acac)(mba) (7), Ge(tmhd)(mpa) (8), Ge(tmhd)(mdpa) (9), Ge(tmhd)(empa) (10), Ge(tmhd)(edpa) (11), and Ge(tmhd)(mba) (12). Among these complexes, Ge(acac)Cl has already been reported, but in this paper, the crystal structure was established and the molecular structures of representative complexes were established by X-ray crystallography.⁵⁹ All complexes were characterized by using nuclear magnetic resonance (NMR) spectroscopy, Fourier transform infrared spectroscopy (FT-IR), thermogravimetric analysis (TGA), elemental analysis (EA), and mass spectrometry (MS). Complexes 1 and 7, which exhibited monomeric structures, were further characterized using X-ray crystallography.

RESULTS AND DISCUSSION

Synthesis. To investigate the properties of the germanium complexes, we synthesized several germanium complexes

Table 2. Physical Properties of Complexes 1–12

| complex | formula | molecular weight (g/mol) | onset temperature of 1 wt % loss (°C) | temperature at 50 wt % loss (°C) | nonvolatile residual mass (%) |
|---------|---|--------------------------|---------------------------------------|----------------------------------|-------------------------------|
| 1 | C ₃ H ₇ O ₂ ClGe | 207.93 | 103 | 185 | 3.4 |
| 2 | C ₁₁ H ₁₉ O ₂ ClGe | 292.03 | 104 | 178 | |
| 3 | C ₉ H ₁₅ NO ₄ Ge | 275.02 | 101 | 399 | 47.1 |
| 4 | C ₁₁ H ₁₉ NO ₄ Ge | 303.05 | 94 | 169 | 15.4 |
| 5 | C ₁₁ H ₁₉ NO ₄ Ge | 303.05 | 107 | 194 | 32.2 |
| 6 | C ₁₂ H ₂₁ NO ₄ Ge | 317.07 | 102 | 178 | 18.1 |
| 7 | C ₁₃ H ₁₅ NO ₄ Ge | 323.02 | 136 | 285 | 42.9 |
| 8 | C ₁₅ H ₂₇ NO ₄ Ge | 359.12 | 108 | 201 | 7.1 |
| 9 | C ₁₇ H ₃₁ NO ₄ Ge | 387.15 | 113 | 189 | 9.7 |
| 10 | C ₁₇ H ₃₁ NO ₄ Ge | 387.14 | 120 | 199 | 4.6 |
| 11 | C ₁₈ H ₃₃ NO ₄ Ge | 401.16 | 121 | 198 | 2.0 |
| 12 | C ₁₉ H ₂₇ NO ₄ Ge | 407.12 | 129 | 234 | 12.5 |

utilizing β -diketonate and *N*-alkoxy carboxamide ligands. In addition to the *N*-alkoxy carboxamide ligands that performed well in our previous study, we aimed to develop compounds with higher volatility using β -diketonate, enhancing the overall volatility of the complex. All of the complexes in this study were prepared using a salt-elimination process, as shown in Scheme 1. The intermediate molecules, Ge(acac)Cl (**1**) and Ge(tmhd)Cl (**2**), were synthesized by reacting the starting compound GeCl₂-dioxane with one equivalent of a sodium salt of β -diketonate in tetrahydrofuran (THF) at ambient temperatures. To synthesize new germanium complexes, the Cl atom of the compound was substituted with an *N*-alkoxy carboxamide ligand. The final products were purified by sublimation (complex **1**), distillation (complex **2**), and crystallization from a saturated hexane solution (complexes **3**–**12**) with good-to-excellent yields of 87–98%. However, only the colorless crystals of complexes **1** and **7** were further investigated for their structural properties by using single-crystal X-ray diffraction, whereas the other complexes could not be structurally characterized because of their unsuitable crystallinity. These two complexes were identified as having a monomeric structure and are discussed further below. They were observed to be highly stable under inert argon gas conditions; however, they were sensitive to air and moisture. They exhibited high solubility in organic solvents, such as hexane, toluene, diethyl ether, and THF.

NMR Study. A series of synthesized germanium complexes were characterized by NMR spectrometry using benzene-*d*₆ as the solvent and reference at room temperature. Complexes **1** and **2** were identified by the peak of each functional group as methyl (**1**), *tert*-butyl (**2**), and the β -CH of each corresponding β -diketonate ligand. Complex **1** displayed the CH₃ peak at 1.45 ppm and the β -CH peak at 5.02 ppm, respectively, as a singlet. Complex **2** revealed the same shift patterns as **1**. Compound **2** exhibited an upfield shifted *tert*-butyl peak at 1.00 ppm with a singlet and a downfield shifted β -CH peak of 6.01 ppm compared to Na(tmhd), which has 1.21 and 5.78 ppm (Figures S1–S4). The spectra of complexes **3**, **4**, **7**, **8**, **9**, and **12** appeared at the peaks of O-methyl at δ_{H} = 3.82, 3.82, 3.92, 3.83, 3.84, and 3.93 ppm, respectively. The CH₂ protons from O-ethyl peaks of **5**, **6**, **10**, and **11** were shown at δ_{H} = 4.23, 4.20, 4.23, and 4.20 ppm as a quartet. Also, the phenyl of complexes **7** and **12** displayed the same signal range as the multiplet at δ_{H} = 7.00–7.15 ppm. All compounds that have *N*-alkoxy carboxamide ligands exhibited the downfield shifted alkyl peaks and upfield shifted β -CH peaks of β -diketonate

ligands compared to complexes **1** and **2** (shown in Figures S5–S24).

FT-IR Spectroscopy. The most prominent peaks of complexes **1** and **2** are the alkyl and C=O functional groups from the β -diketonate ligand. The spectrum of complex **1** showed methyl peaks at ν = 2963–3109 cm⁻¹ as weak stretching and the C=O peaks at 1541 cm⁻¹ with strong stretching. The FT-IR spectrum of complex **2** displayed the strong stretches of *tert*-butyl at 2871–2969 cm⁻¹ and the strong stretching of the C=O peaks at 1533 cm⁻¹.⁶⁰ The stretching frequencies of the C=N bond of the *N*-alkoxy carboxamide observed at ν = 1604 (**3**), 1618 (**4**), 1690 (**5**), 1658 (**6**), 1658 (**7**), 1606 (**8**), 1595 (**9**), 1606 (**10**), 1598 (**11**), and 1599 cm⁻¹ (**12**) exhibited different wavenumbers compared to each sodium salt of the corresponding ligands. For complexes **7** and **12** containing the aromatic and alkyls, the C–H stretches overlapped in the range of ν = 2899–3064 cm⁻¹ (**7**) and 2814–3099 cm⁻¹ (**12**), respectively.

TGA

The TGA results of all of the complexes demonstrated an interesting tendency, indicating that the alkyl group of the β -diketonates influences the thermal stability of the compound. We designed new heteroleptic germanium compounds using a combination of β -diketonate ligands containing *N*-alkoxy carboxamide ligands, which were previously investigated to further improve the volatility of the Ge precursors.⁵⁵ TGA was performed to confirm the thermal stability, volatility, and decomposition temperatures of the synthesized Ge complexes. All thermal investigations were conducted at temperatures ranging from room temperature to 500 °C under inert argon gas conditions (it is shown in Table 2). Overall, TGA plots of new germanium complexes exhibited similar thermal behaviors where weight loss occurred in a single step within a range of approximately 100–250 °C, except compounds **3** and **5**, which exhibited a multistep decomposition. The final residual masses of the synthesized compounds **1**–**12** were obtained as 3.4% (**1**), 0% (**2**), 47.1% (**3**), 15.4% (**4**), 32.2% (**5**), 18.1% (**6**), 42.9% (**7**), 7.1% (**8**), 9.7% (**9**), 4.6% (**10**), 2.0% (**11**), and 12.5% (**12**). The thermogram of complex **1** with chloride represented 93% weight loss at 210 °C, followed by 3.4% of the final residue at 500 °C, demonstrating excellent volatilization properties. In contrast, the thermal stability of compounds **3**–**7** shows a poor correlation with the carboxamide ligands. The TGA results demonstrated that Ge(acac)(*N*-alkoxy carboxamide) was less volatile than the

homoleptic $\text{Ge}(\text{N-alkoxy carboxamide})_2$.⁵⁵ As shown in Figures 1 (acac) and 2 (tmhd), the lowest residue acac-

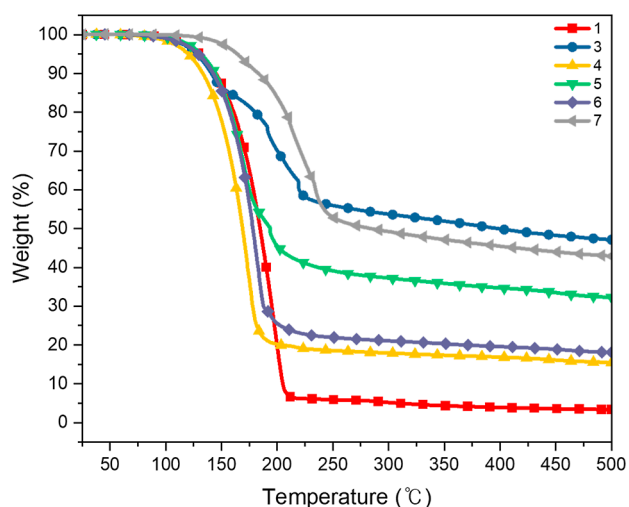


Figure 1. TGA curves of germanium complexes **1** and **3–7** containing the acac ligand. All thermal investigations were conducted at temperatures ranging from room temperature to 500 °C with a temperature ramp of 20 K/min under inert argon gas conditions.

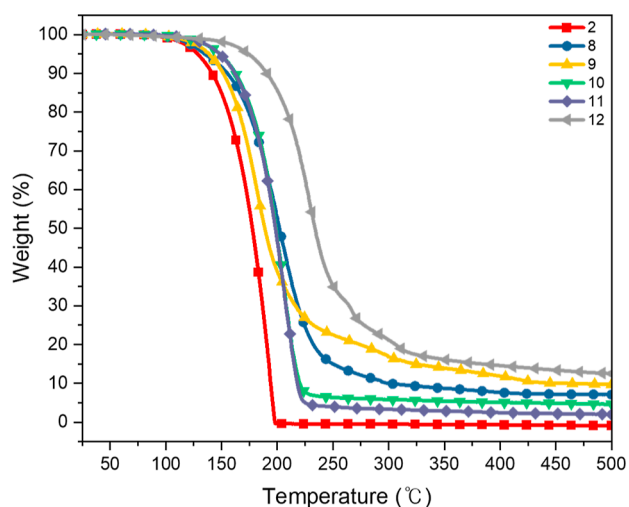


Figure 2. TGA curves of germanium complexes **2** and **8–12** containing tmhd ligand. All thermal investigations were conducted at temperatures ranging from room temperature to 500 °C with a temperature ramp of 20 K/min under inert argon gas conditions.

containing compound **4** exhibited lower volatility than the highest residue tmhd-containing complex **12**, indicating that the tmhd ligand complexes exhibited better thermal properties than the acac ligand complexes, regardless of the *N*-alkoxy carboxamide ligands. In addition, in the case of $\text{Ge}(\text{tmhd})(\text{N-alkoxy carboxamide})$ -type complexes **8–12**, the 1% weight loss onset temperature depended on the molecular weight of the germanium complexes. That is, complex **12** has a higher onset temperature of 129 °C. Interestingly, complex **2** was completely volatilized at <200 °C without thermal decomposition with no final residue. Therefore, it should be noted that liquid compound **2** exhibits the highest volatility and thermal stability among the newly synthesized germanium complexes, demonstrating its potential as a precursor for germanium-containing thin films during the ALD process.

X-ray Crystallography. The newly synthesized germanium complexes were recrystallized to grow X-ray-quality single crystals in a saturated hexane solution at room temperature to investigate the solid-phase conformer. Complex **1** coordinated with two oxygen atoms of the acac ligand and one chlorine. Also, the germanium atom has a lone pair, which makes it a distorted molecular structure due to electron pair repulsion. As a result of this, the structure of **1** has a distorted trigonal pyramidal structure with a monomer geometry, as shown in Figure 3. It was defined as the orthorhombic crystal

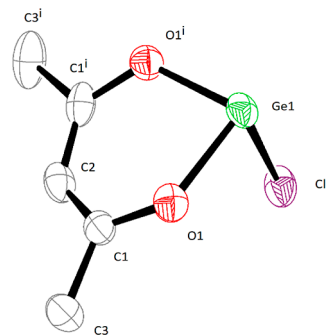


Figure 3. Molecular structure of complex **1** with thermal ellipsoids at the 50% probability level. All hydrogen atoms are omitted for clarity (green, germanium; red, oxygen; purple, chlorine; and gray, carbon).

system with the *Pmna* space group and displayed six molecules in a unit cell. The structure has a type of GeX_3E ($\text{X} = \text{ligands}$; $\text{E} = \text{lone pair electron}$).⁶¹ The bond angles of the O–Ge–Cl bond revealed 93.14(7)°, and the angle of the $\text{O–Ge–O}'$ bond showed 91.22(15)°. The bond lengths of germanium and two oxygens were the same as 1.927(3) Å, respectively, and the length with chlorine was 2.275(13) Å (shown in Table 3). The

Table 3. Selected Bond Lengths (Å) and Angles (deg) of Complex **1**

| bond length (Å) | | bond angles (deg) | |
|-----------------|-----------|-------------------|-----------|
| Ge–Cl | 2.276(13) | O–Ge–Cl | 93.14(7) |
| Ge–O | 1.927(3) | O–Ge–O' | 91.22(15) |

Ge–Cl in complex **1** has a longer distance than those of reported tetravalent complexes such as $\text{Cl}_3\text{Ge}[\text{OCHMeC}(\text{O})\text{NR}^1]$, $\text{Cl}_2\text{MeGe}[\text{OCHR}^2\text{C}(\text{O})\text{NMe}]$, $\text{Ge}(\text{EthdH}_1)_2\text{Cl}_2$, and $\text{Cl}_2\text{Ge}[\text{OCH}_2\text{C}(\text{O})\text{NR}^3]$ ($\text{R}^1 = \text{Me}_2$, $(\text{CH}_2)_4$, $(\text{CH}_2)_5$; $\text{R}^2 = (\text{CH}_2)_5$, Me, H; $\text{R}^3 = (\text{CH}_2\text{CH}_2)_2\text{O}$, $(\text{CH}_2)_5$) with 2.139(5)–2.270(6) Å, but is within the range of bond length.^{52,62–64} $\text{Ge}(\text{II})\text{–Cl}$ bond lengths are longer than the $\text{Ge}(\text{IV})$ bond lengths because the $\text{Ge}(\text{II})$ ion is slightly larger than the $\text{Ge}(\text{IV})$ ion. To investigate the solid-state structures of the newly designed complexes, we applied an mba ligand with good packing ability by a phenyl group. The germanium of complex **7** formed four bonds with four oxygen atoms like GeX_4E and showed a twin structure with a distorted seesaw geometry. It is a monomer and has a monoclinic crystal system and space group of *P2(1)/c*. The central axis of **7** is O1–Ge–O4 (151.74(10)°), and the bond angle of the equatorial, O2–Ge–O3 , was 91.12(11)° (it is shown in Figure 4 and Table 4). The bond lengths of germanium and each corresponding oxygens of oxygens O1 to O4 were 2.003(3), 1.950(3), 1.904(3), and 2.435(3) Å, respectively. This indicated that the bond length of Ge–O4 displayed the longest and Ge–O3 of

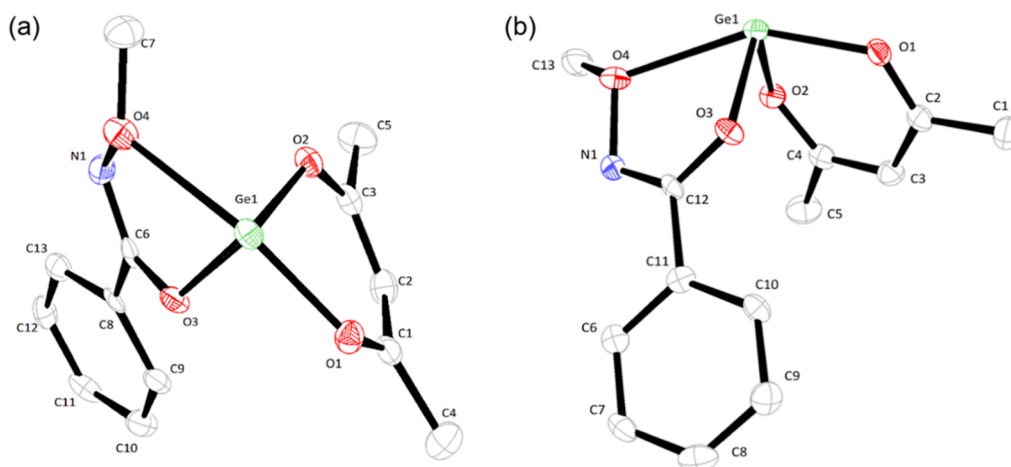


Figure 4. (a) Top view and (b) side view of molecular structures of complex 7 with thermal ellipsoids at the 50% probability level. All hydrogen atoms are omitted for clarity (green, germanium; red, oxygen; blue, nitrogen; and gray, carbon).

Table 4. Selected Bond Lengths (Å) and Angles (deg) of Complex 7

| bond length (Å) | | bond angles (deg) | |
|-----------------|----------|-------------------|------------|
| Ge–O1 | 2.003(3) | O1–Ge–O2 | 88.15(11) |
| Ge–O2 | 1.950(3) | O1–Ge–O3 | 86.66(12) |
| Ge–O3 | 1.904(3) | O1–Ge–O4 | 151.74(10) |
| Ge–O4 | 2.435(3) | O2–Ge–O3 | 91.12(11) |
| | | O2–Ge–O4 | 77.28(10) |
| | | O3–Ge–O4 | 69.79(10) |

1.904(3) Å was shorter than other bonds. This is a different result from the previous study using the same ligand.⁵⁵ In addition, 7 exhibited a longer Ge–O bond than complex 1 which has a distance of 1.927(3) without an *N*-alkoxy carboxamide ligand.

ALD of the GeO₂ Film. In investigating the ALD process, complex 2, namely, Ge(tmhd)Cl, was employed as the precursor, given its liquid state and superior vapor pressure, along with its commendable stability among the synthesized complexes. Figure 5a shows the change in the growth per cycle (GPC) according to the injection time of the Ge precursor and H₂O₂. The temperature of the substrate was maintained at 300 °C, and the purge times of the Ge precursor and H₂O₂ were fixed at 10 and 15 s, respectively. In both cases, the GPC saturated to approximately 0.3 Å/cycle with increasing injection time, demonstrating the ALD-specific self-limiting

behavior. Therefore, in subsequent experiments, the injection times of the Ge precursor and H₂O₂ were fixed at 6 and 3 s, respectively. Notably, when the H₂O₂ injection time was 0 s, the film did not grow, indicating that the CVD-like growth through thermal decomposition of the Ge precursor did not occur. Similarly, when the Ge precursor injection time was set to 0 s, no thin film growth was observed, offering supporting evidence that H₂O₂ did not induce oxidation of the Si substrate. Moreover, an investigation into the growth rate variations concerning the precursor and H₂O₂ purge time was conducted separately, revealing the presence of self-limiting behavior at each purge time equal to or exceeding 5 s (Figure S37). The possibility of oxidation of Ge by H₂O₂ was also confirmed by the lack of reaction with the Ge precursor and the absence of an increase in the thickness of the thin film. This finding suggests that the oxidation of Ge occurs only by H₂O₂ (data not shown). Figure 5b shows the change in the thickness of the thin film as a function of the cycle number. As the number of cycles increased, the thickness increased linearly and the saturated GPC obtained from the slope was 0.27 Å/cycle. Here, the intercept value of the fitting line was approximately 5 Å, indicating accelerated growth characteristics facilitated by the substrate during the initial stage of growth. This phenomenon was also evident in the layer density variation according to the Ge cycle number, where the intercept value of the fitting line was approximately 0.21 μg/

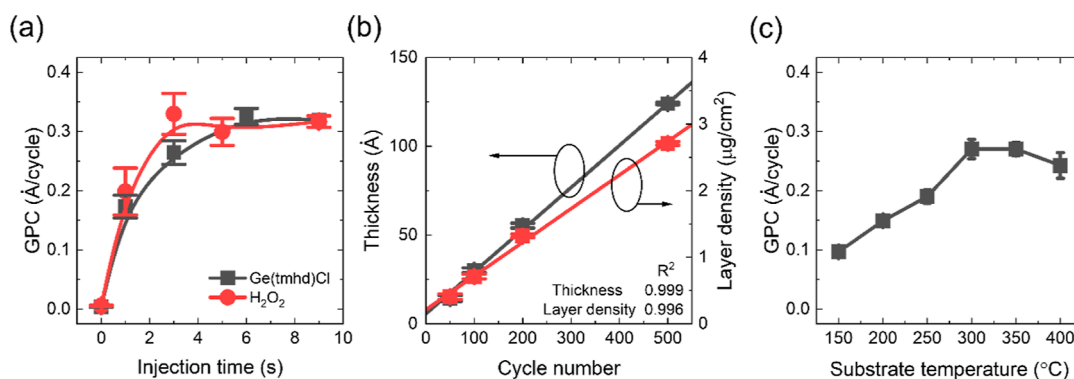


Figure 5. Influence of the process conditions on the growth of GeO₂, namely, (a) Ge precursor and oxidant supply, (b) ALD cycle number, and (c) substrate temperature.

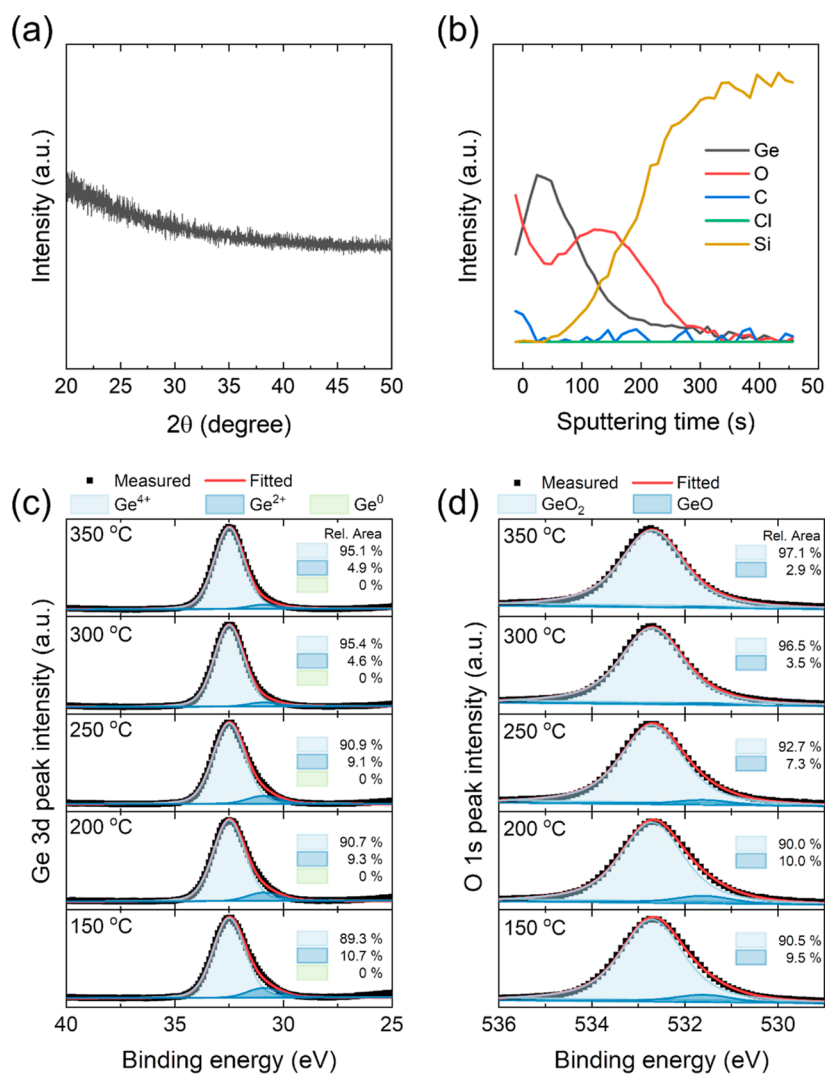


Figure 6. Chemical and elemental characterization of GeO₂ thin films based on (a) glancing angle X-ray diffraction (GAXRD) patterns, (b) Auger electron spectroscopy (AES) depth profile, (c) Ge 3d X-ray photoelectron spectroscopy (XPS) spectra, and (d) O 1s XPS spectra.

cm², which showed that the early ALD cycles promoted the formation of the Ge layer through reactions between the Si substrate and the Ge precursor. The obtained densities, calculated using the thickness and area density, were found to be 2.87, 2.35, 2.39, and 2.18 g/cm³ for samples deposited with 50, 100, 200, and 500 cycles, respectively. These values represent 67 to 51% of the bulk density. While these densities may be considered somewhat low, they are consistent with previous GeO_x ALD results reported in the literature. The observed low density is likely attributed to factors such as low crystallinity and stoichiometry within the thin films.⁸ Figure 5c shows the effect of the substrate temperature on the GPC, where the GPC maintained a consistent level of 0.27 Å/cycle at temperatures ranging from 300 to 350 °C. The GPC decreased at temperatures <300 °C owing to the insufficient thermal energy for the ligand exchange reaction; it also decreased at temperatures >350 °C owing to the accelerated desorption of adsorbates. As listed in Table 1, the GPC was similar to or lower than the previously reported results; however, the film can be formed without the O₃ oxidant, which requires additional facilities. In addition, the film can be synthesized at a higher temperature than other precursors by preventing desorption or decomposition more effectively.^{3,13,52}

GAXRD analysis was conducted with the as-deposited 12 nm-thick GeO₂ film grown at 300 °C (Figure 6a). The GeO₂ film did not exhibit any characteristic diffraction peaks, indicating that it was formed in an amorphous phase, which, in turn, ensures its notable solubility in water. This result is reasonable because GeO₂ is well-known as a good glass former.³⁰ As shown in the AES depth profile (Figure 6b), chlorine impurity in the thin film grown at 300 °C was below the detection limit of the facility (<0.1%), indicating that the chlorine ligand is completely removed from the Ge precursor by the H₂O₂. The AES depth profile exhibited a carbon impurity concentration with a noise level comparable to that of the Si substrate. However, XPS analysis revealed the presence of an impurity at approximately 7 atom % concentration (Figures S38 and S39). The discrepancy in carbon concentration observed between AES and XPS measurements could stem from several factors, with a possible contributing factor being the inadequate removal of carbon residues on the surface of the XPS sample. Figure 6c and d illustrates the results of the XPS analysis, which determined the chemical bonding state of a 5 nm-thick GeO₂ film. Figure 6c shows the Ge 3d core-level spectra of the films deposited at a substrate temperature range of 150–350 °C. The peaks exhibited at

29.1, 30.9, and 32.5 eV correspond to the chemical bonding states of Ge⁰, Ge²⁺, and Ge⁴⁺, respectively.⁶⁵ As the deposition temperature increased, the peak area of Ge⁴⁺ increased from 89.3 to 95.1%, whereas that of Ge²⁺ decreased from 10.7 to 4.9%. This was attributed to the activation of the ligand-exchange reaction with an increasing temperature, which suppressed the generation of the metastable GeO phase while promoting the generation of the stable GeO₂ phase. However, the Ge⁰ peak did not exist at all deposition temperatures, indicating that elemental Ge, which could be formed owing to thermal decomposition, did not exist in the thin film. The same trend was observed in the O 1s core-level spectra (Figure 6d). The peaks exhibited at 531.6 and 532.7 eV correspond to the chemical bonding states of GeO and GeO₂, respectively.⁶⁶ As the deposition temperature increased, the peak area of GeO₂ increased from 90.5 to 97.1%, whereas that of GeO decreased from 9.5 to 2.9%, confirming that it was closer to the stoichiometric GeO₂ film. In Figure S40, the XPS survey spectra reveal the presence of both Ge and O within the thin film and also demonstrate changes in the C content before and after etching.

EXPERIMENTAL SECTION

NMR spectra were recorded using Bruker 400 and 500 MHz spectrometers with C₆D₆ as the solvent and standard.⁶⁷ FT-IR spectra were obtained using a Nicolet NEXUS FT-IR spectrophotometer with a 4 mm KBr window or KBr pellets. KBr pellets of the samples were prepared by using a standard pellet technique inside a glovebox. TGA was conducted by using a NETZSCH TG 209 F3TG instrument under inert argon gas conditions. Single-crystal structures were confirmed by using a Bruker SMART APEX II X-ray diffractometer. EA was performed using a Thermo Scientific FLASH 2000 organic elemental analyzer. MS was conducted in electron ionization (EI) and fast atom bombardment (FAB) modes using a JEOL JMS-700 high-resolution mass spectrometer (HR-MS). The sodium salt ligand of β -diketonate and *N*-alkoxy carboxamide were prepared using NaH. All reactions were performed under inert dry conditions using an argon-filled glovebox. Hexane and THF were purified using an Innovative Technology PSMD-4 solvent purification system. All chemicals were purchased from Aldrich, TCI, or STREM and used as received.

General Procedure of the Synthesis of New Germanium Complexes. *Preparation of Ge(β -diketonate)-Cl.* One equivalent sodium salt of the β -diketonate ligand was gradually added portionwise to a solution of GeCl₂·dioxane (3.0 g, 12.95 mmol) in THF (30 mL) under ambient conditions. Thereafter, the reaction mixture was stirred constantly for 15 h. After the completion of the reaction, the mixture evaporated to dryness. Hexane was subsequently added, the mixture was filtered to remove salts, and the filtrate was evaporated in vacuo to obtain the crude product.

Ge(acac)Cl (1). Na(acac) (1.6 g, 12.95 mmol) was used to prepare complex 1. The pure white solid product was obtained through sublimation (40 °C/0.3 Torr). The compound can be obtained as a colorless crystalline solid by recrystallization from a saturated hexane solution at room temperature. Yield: 2.63 g (98%). mp 61 °C. ¹H NMR (500 MHz, C₆D₆): δ (ppm): δ 5.02 (s, 1H, β -CH), 1.45 (s, 6H, CH₃). ¹³C NMR (101 MHz, C₆D₆): δ (ppm): δ 190.6 (OCCH₃), 103.4 (β -CH), 26.8 (OCCH₃). Anal. calcd for C₅H₇O₂ClGe: C, 28.98; H, 3.41. Observed: C, 28.99; H, 3.41. HR-MS (EI): [M]⁺ calcd (C₅H₇O₂ClGe) 207.9346. Observed: 207.9363. FT-IR (KBr,

cm⁻¹): 3109 (w), 3038 (w), 2963 (w), 1540 (s), 1425 (m), 1336 (s), 1289 (m), 1019 (m), 945 (m), 817 (m).

Ge(tmhd)Cl (2). Na(tmhd) (2.67 g, 12.95 mmol) was used to prepare complex 2. The pure colorless liquid product was obtained through distillation (80 °C/0.3 Torr). Yield: 3.66 g (97%). ¹H NMR (500 MHz, C₆D₆): δ (ppm): δ 6.01 (s, 1H, β -CH), 1.00 (s, 18H, C(CH₃)₃). ¹³C NMR (101 MHz, C₆D₆): δ (ppm): δ 200.6 (OCC), 94.7 (β -CH), 41.2 (OCC), 27.6 (C(CH₃)₃). Anal. calcd for C₁₁H₁₉O₂ClGe: C, 45.35; H, 6.57. Observed: C, 45.38; H, 6.58. HR-MS (EI): [M]⁺ calcd (C₁₁H₁₉O₂ClGe) 292.0285. Observed: 292.0285. FT-IR (KBr, cm⁻¹): 2969 (s), 2935 (w), 2908 (w), 1533 (s), 1462 (w), 1366 (m), 1329 (s), 1250 (m), 1220 (m), 1149 (m), 961 (m), 875 (m).

*Preparation of Ge(β -diketonate)(*N*-alkoxy carboxamide).* A hexane solution (10 mL) of the sodium salt of the *N*-alkoxy carboxamide ligand was added dropwise to the Ge(β -diketonate)Cl complex in hexane (30 mL) at room temperature. The reaction mixture was constantly stirred for 15 h. After the reaction was complete, the mixture was filtered to remove NaCl salts, and the volatiles were removed from the filtrate in vacuo to obtain the products. All crude compounds were purified as pure complexes through crystallization from a saturated hexane solution at room temperature. Crystallization of the synthesized compound was attempted under various experimental conditions. Among them, the best way to obtain crystals was to saturate the complexes with 50, 80, and 100% hexane solvents in an Ar-filled glovebox and slowly evaporate.

Ge(acac)(mpa) (3). Ge(acac)Cl (1) (0.5 g, 2.41 mmol) and Na(mpa) (0.3 g, 2.41 mmol) were used to prepare complex 3 as a low-melting solid. Yield: 0.57 g (87%). ¹H NMR (500 MHz, C₆D₆): δ (ppm): δ 5.07 (s, 1H, β -CH), 3.82 (s, 3H, OCH₃), 2.22 (q, *J* = 7.5 Hz, 2H, CH₂), 1.59 (s, 6H, CH₃), 1.07 (t, *J* = 7.5 Hz, 3H, CH₃). ¹³C NMR (101 MHz, C₆D₆): δ (ppm): δ 189.4 (OCCH₃), 163.9 (OCN), 101.8 (β -CH), 59.7 (OCH₃), 26.8 (OCCH₃), 25.1 (CH₂), 11.3 (CH₃). Anal. calcd for C₉H₁₅NO₄Ge: C, 39.47; H, 5.52; N, 5.11. Observed: C, 39.34; H, 5.80; N, 5.25. HR-MS (FAB): [M]⁺ calcd (C₉H₁₅NO₄Ge) 275.0213. Observed: 276.1196. FT-IR (KBr, cm⁻¹): 2972 (w), 2937 (w), 1604 (m), 1570 (s), 1530 (s), 1463 (w), 1434 (w), 1351 (s), 1280 (m), 1263 (w), 1188 (w), 1051 (s), 1022 (m), 1001 (w), 853 (w).

Ge(acac)(mdpa) (4). Ge(acac)Cl (1) (0.5 g, 2.41 mmol) and Na(mdpa) (0.37 g, 2.41 mmol) were used to prepare complex 4 as a low-melting solid. Yield: 0.67 g (92%). ¹H NMR (500 MHz, C₆D₆): δ (ppm): δ 5.08 (s, 1H, β -CH), 3.82 (s, 3H, OCH₃), 1.61 (s, 6H, CH₃), 1.28 (s, 9H, C(CH₃)₃). ¹³C NMR (101 MHz, C₆D₆): δ (ppm): δ 189.3 (OCCH₃), 168.1 (OCN), 101.9 (β -CH), 59.7 (CH₃), 36.0 (C(CH₃)₃), 28.2 (C(CH₃)₃), 26.7 (OCCH₃). Anal. calcd for C₁₁H₁₉NO₄Ge: C, 43.76; H, 6.34; N, 4.64. Observed: C, 42.80; H, 6.19; N, 4.01. HR-MS (EI): [M]⁺ calcd (C₁₁H₁₉NO₄Ge) 303.0526. Observed: 303.0527. FT-IR (KBr, cm⁻¹): 2973 (s), 2936 (s), 2901 (s), 2868 (m), 2814 (w), 1548 (s), 1481 (s), 1435 (s), 1359 (s), 1282 (s), 1224 (w), 1188 (s), 1052 (s), 1024 (s), 944 (m), 864 (m), 796 (m).

Ge(acac)(empa) (5). Ge(acac)Cl (1) (0.5 g, 2.41 mmol) and Na(empa) (0.37 g, 2.41 mmol) were used to prepare complex 5 as a low-melting solid. Yield: 0.64 g (88%). ¹H NMR (500 MHz, C₆D₆): δ (ppm): δ 5.09 (s, 1H, β -CH), 4.23 (q, *J* = 7.1 Hz, 2H, OCH₂), 2.65 (hept, *J* = 6.9 Hz, 1H, CH), 1.61 (s, 6H, CH₃), 1.35 (t, *J* = 7.1 Hz, 3H, CH₃), 1.16 (d, *J* = 6.9 Hz, 6H, C(CH₂)₂). ¹³C NMR (101 MHz, C₆D₆): δ

(ppm): δ 189.3 (OCCH₃), 165.9 (OCN), 101.8 (β -CH), 68.9 (CH₂), 31.6 (C(CH₂)₂), 26.7 (OCCH₃), 20.3 (C(CH₂)₂), 15.3 (CH₃). Anal. calcd for C₁₁H₁₉NO₄Ge: C, 43.76; H, 6.34; N, 4.64. Observed: C, 43.37; H, 6.40; and N, 4.62. HR-MS (EI): [M]⁺ calcd (C₁₁H₁₉NO₄Ge) 303.0526. Observed: 303.0527. FT-IR (KBr, cm⁻¹): 2976 (s), 2931 (m), 2901 (m), 2870 (m), 1579 (s), 1532 (s), 1482 (m), 1457 (m), 1438 (m), 1359 (s), 1328 (s), 1282 (m), 1224 (w), 1191 (s), 1128 (w), 1092 (w), 1052 (s), 1023 (s), 960 (w), 940 (m), 902 (w), 864 (w).

Ge(acac)(edpa) (6). Ge(acac)Cl (1) (0.5 g, 2.41 mmol) and Na(edpa) (0.4 g, 2.41 mmol) were used to prepare complex 6 as a low-melting solid. Yield: 0.73 g (96%). ¹H NMR (400 MHz, C₆D₆): δ (ppm): δ 5.12 (s, 1H, β -CH), 4.20 (q, *J* = 7.1 Hz, 2H, CH₂), 1.63 (s, 6H, CH₃), 1.33 (t, *J* = 7.0 Hz, 3H, CH₃), 1.25 (s, 9H, C(CH₃)₃). ¹³C NMR (101 MHz, C₆D₆): δ (ppm): δ 189.2 (OCCH₃), 167.6 (OCN), 101.8 (β -CH), 69.0 (CH₂), 36.2 (C(CH₃)₃), 28.2 (C(CH₃)₃), 26.7 (OCCH₃), 15.3 (CH₃). Anal. calcd for C₁₂H₂₁NO₄Ge: C, 45.62; H, 6.70; N, 4.43. Observed: C, 44.91; H, 6.66; N, 4.46. HR-MS (FAB): [M]⁺ calcd (C₁₂H₂₁NO₄Ge) 317.0682. Observed: 318.0763. FT-IR (KBr, cm⁻¹): 2976 (s), 2931 (m), 2901 (m), 2870 (m), 1579 (s), 1532 (s), 1482 (m), 1359 (s), 1282 (m), 1191 (s), 1128 (m), 1092 (m), 1052 (s), 1023 (s), 925 (m), 864 (w), 787 (w).

Ge(acac)(mba) (7). Ge(acac)Cl (1) (0.5 g, 2.41 mmol) and Na(mba) (0.42 g, 2.41 mmol) were used to prepare complex 7 as a low-melting solid. The obtained crude compound was refined into a pure colorless crystalline solid complex by recrystallization from a saturated hexane solution at room temperature. Yield: 0.76 g (98%). mp 82 °C. ¹H NMR (500 MHz, C₆D₆): δ (ppm): δ 8.21–8.11 (m, 2H, Ph), 7.14–6.99 (m, 3H, Ph), 5.03 (s, 1H, β -CH), 3.92 (s, 3H, OCH₃), 1.56 (s, 6H, CH₃). ¹³C NMR (101 MHz, C₆D₆): δ (ppm): δ 189.6 (OCCH₃), 159.1 (OCN), 133.4 (Ph), 129.7 (Ph), 128.2 (Ph), 127.2 (Ph), 102.0 (β -CH), 60.5 (CH₃), 26.7 (OCCH₃). Anal. calcd for C₁₃H₁₅NO₄Ge: C, 48.51; H, 4.70; N, 4.35. Observed: C, 47.97; H, 4.70; N, 4.30. HR-MS (EI): [M]⁺ calcd (C₁₃H₁₅NO₄Ge) 323.0213. Observed: 323.0204. FT-IR (KBr, cm⁻¹): 3199 (w), 3064 (w), 2965 (w), 2936 (w), 2899 (w), 1658 (w), 1561 (s), 1532 (s), 1437 (w), 1345 (s), 1284 (w), 1189 (w), 1116 (m), 1050 (m), 1025 (m), 924 (w), 799 (m).

Ge(tmhd)(mpa) (8). Ge(tmhd)Cl (2) (0.5 g, 1.72 mmol) and Na(mpa) (0.22 g, 1.72 mmol) were used to prepare complex 8 as a low-melting solid. Yield: 0.56 g (90%). ¹H NMR (500 MHz, C₆D₆): δ (ppm): δ 5.91 (s, 1H, β -CH), 3.83 (s, 3H, OCH₃), 2.17 (q, *J* = 7.6 Hz, 2H, CH₂), 1.09 (s, 18H, C(CH₃)₃), 1.06 (t, 3H, CH₃). ¹³C NMR (101 MHz, C₆D₆): δ (ppm): δ 199.4 (OCC), 92.7 (β -CH), 59.6 (OCN), 41.2 (OCC), 28.3 (OCH₃), 27.9 (C(CH₃)₃), 24.9 (CH₂), 11.2 (CH₃). Anal. calcd for C₁₅H₂₇NO₄Ge: C, 50.32; H, 7.60; N, 3.91. Observed: C, 50.25; H, 7.75; N, 3.75. HR-MS (FAB): [M]⁺ calcd (C₁₅H₂₇NO₄Ge) 359.1152. Observed: 360.1200. FT-IR (KBr, cm⁻¹): 2967 (s), 2937 (m), 2906 (m), 2874 (w), 1606 (m), 1545 (s), 1510 (s), 1464 (m), 1344 (s), 1287 (m), 1264 (m), 1220 (m), 1189 (w), 1147 (m), 1058 (s), 1002 (w), 961 (w), 873 (m).

Ge(tmhd)(mdpa) (9). Ge(tmhd)Cl (2) (0.5 g, 1.72 mmol) and Na(mdpa) (0.26 g, 1.72 mmol) were used to prepare complex 9 as a low-melting solid. Yield: 0.58 g (88%). ¹H NMR (500 MHz, C₆D₆): δ (ppm): δ 5.91 (s, 1H, β -CH), 3.84 (s, 3H, OCH₃), 1.26 (s, 9H, C(CH₃)₃), 1.09 (s, 18H, C(CH₃)₃). ¹³C NMR (101 MHz, C₆D₆): δ (ppm): δ 199.2

(OCC), 167.8 (OCN), 92.7 (β -CH), 59.7 (CH₃), 41.2 (OCC), 36.0 (C(CH₃)₃), 28.3 (C(CH₃)₃, mdpa), 28.0 (C(CH₃)₃, tmhd). Anal. calcd for C₁₇H₃₁NO₄Ge: C, 52.89; H, 8.09; N, 3.63. Observed: C, 52.56; H, 8.16; N, 3.54. HR-MS (EI): [M]⁺ calcd (C₁₇H₃₁NO₄Ge) 387.1465. Observed: 387.1464. FT-IR (KBr, cm⁻¹): 2967 (s), 2935 (m), 2905 (m), 2869 (w), 1595 (w), 1547 (s), 1509 (s), 1481 (w), 1393 (w), 1365 (m), 1344 (s), 1323 (m), 1225 (w), 1189 (m), 1146 (w), 1056 (m), 961 (w), 874 (w).

Ge(tmhd)(empa) (10). Ge(tmhd)Cl (2) (0.5 g, 1.72 mmol) and Na(empa) (0.263, 1.72 mmol) were used to prepare complex 10 as a low-melting solid. Yield: 0.61 g (92%). ¹H NMR (500 MHz, C₆D₆): δ (ppm): δ 5.91 (s, 1H, β -CH), 4.22 (q, *J* = 7.0 Hz, 2H, OCH₂), 2.60 (hept, *J* = 6.9 Hz, 1H, CH), 1.36 (t, *J* = 7.5 Hz, 3H, CH₃), 1.13 (d, *J* = 6.9 Hz, 6H, C(CH₂)₂), 1.10 (s, 18H, C(CH₃)₃). ¹³C NMR (101 MHz, C₆D₆): δ (ppm): δ 199.2 (OCC), 165.6 (OCN), 92.7 (β -CH), 68.9 (CH₂), 41.2 (OCC), 31.4 (C(CH₂)₂), 27.9 (C(CH₂)₂), 20.4 (C(CH₃)₃), 15.4 (CH₃). Anal. calcd for C₁₇H₃₁NO₄Ge: C, 52.89; H, 8.09; N, 3.63. Observed: C, 52.82; H, 8.29; N, 3.41. HR-MS (EI): [M]⁺ calcd (C₁₇H₃₁NO₄Ge) 387.1465. Observed: 387.1465. FT-IR (KBr, cm⁻¹): 2967 (s), 2937 (m), 2906 (m), 2874 (w), 2814 (w), 1606 (s), 1545 (s), 1509 (s), 1464 (m), 1344 (s), 1287 (m), 1249 (m), 1220 (w), 1147 (m), 1058 (s), 1002 (w), 961 (w), 874 (m), 803 (w).

Ge(tmhd)(edpa) (11). Ge(tmhd)Cl (2) (0.5 g, 1.72 mmol) and Na(edpa) (0.29 g, 1.72 mmol) were used to prepare complex 11 as a low-melting solid. Yield: 0.62 g (90%). ¹H NMR (500 MHz, C₆D₆): δ (ppm): δ 5.89 (s, 1H, β -CH), 4.20 (q, *J* = 7.0 Hz, 2H, CH₂), 1.33 (t, *J* = 7.1 Hz, 3H, CH₃), 1.23 (s, 9H, C(CH₃)₃), 1.10 (s, 18H, C(CH₃)₃). ¹³C NMR (101 MHz, C₆D₆): δ (ppm): δ 199.1 (OCC), 167.3 (OCN), 92.6 (β -CH), 69.0 (CH₂), 41.2 (OCC), 36.1 (C(CH₃)₃), 28.4 (C(CH₃)₃, edpa), 28.0 (C(CH₃)₃, tmhd), 15.4 (CH₃). Anal. calcd for C₁₈H₃₃NO₄Ge: C, 54.04; H, 8.31; N, 3.50. Observed: C, 54.14; H, 8.47; N, 3.46. HR-MS (FAB): [M]⁺ calcd (C₁₈H₃₃NO₄Ge) 401.1621. Observed: 402.1693. FT-IR (KBr, cm⁻¹): 2968 (s), 2932 (w), 2870 (w), 1598 (w), 1552 (s), 1509 (s), 1482 (w), 1458 (w), 1365 (w), 1344 (s), 1328 (m), 1295 (w), 1250 (w), 1224 (w), 1192 (m), 1146 (m), 1130 (w), 1092 (w), 1053 (m), 961 (w), 874 (w).

Ge(tmhd)(mba) (12). Ge(tmhd)Cl (2) (0.5 g, 1.72 mmol) and Na(mba) (0.3 g, 1.72 mmol) were used to prepare complex 12 as a low-melting solid. Yield: 0.67 g (96%). ¹H NMR (500 MHz, C₆D₆): δ (ppm): δ 8.10–8.12 (m, 2H, Ph), 7.00–7.15 (m, 3H, Ph), 5.90 (s, 1H, β -CH), 3.93 (s, 3H, OCH₃), 1.06 (s, 18H, C(CH₃)₃). ¹³C NMR (101 MHz, C₆D₆): δ (ppm): δ 199.7 (OCC), 158.9 (OCN), 133.5 (Ph), 129.6 (Ph), 128.1 (Ph), 127.1 (Ph), 93.1 (β -CH), 60.4 (CH₃), 41.3 (OCC), 27.9 (C(CH₃)₃). Anal. calcd for C₁₉H₂₇NO₄Ge: C, 56.20; H, 6.70; N, 3.45. Observed: C, 56.48; H, 6.80; N, 3.40. HR-MS (EI): [M]⁺ calcd (C₁₉H₂₇NO₄Ge) 407.1152. Observed: 407.1158. FT-IR (KBr, cm⁻¹): 3058 (w), 2966 (s), 2936 (s), 2904 (m), 2869 (m), 2814 (w), 1599 (m), 1541 (s), 1511 (s), 1461 (m), 1344 (s), 1296 (w), 1249 (m), 1219 (m), 1190 (w), 1147 (m), 1116 (s), 1055 (s), 1027 (m), 961 (m), 923 (m), 874 (s), 805 (m).

ALD of GeO₂ Films. GeO₂ films were grown in a 6 in. scale showerhead-type chamber (Atomic Premium, CN-1) at substrate temperatures ranging from 150 to 400 °C. The Ge precursor, Ge (tmhd)Cl, was bubbled through 200 sccm of Ar gas in the chamber. The H₂O₂ oxidant (34.5%, Samchun Chemicals) was delivered with the aid of 50 sccm of Ar gas by

using the vapor drawing method. Ar gas (400 sccm) was used to purge the unreacted chemicals and byproducts from the vacuum pump. The feeding and purging times were varied to confirm the ALD-specific self-limiting behavior. The temperatures of the Ge precursor canister and delivery line were maintained at 50 and 80 °C, respectively, to achieve sufficient precursor vapor pressure and prevent precursor condensation. The process pressure was maintained at 1 Torr by modulating the throttle valve. Each GeO₂ ALD cycle included four sequential steps: Ge precursor injection, Ge purging, H₂O₂ injection, and H₂O₂ purging. A buffered oxide-etchant-cleaned p-type Si wafer was used as the substrate. The thicknesses of the GeO₂ films were measured through spectroscopic ellipsometry (MG-1000, Nanoview), and the experimental spectra were acquired in the range of 1.45–3.54 eV and measurements were performed in reflection mode at angles of incidence (AOI) of 60°. The spectral analysis was carried out using a stack model consisting of GeO₂ (measured and modeled as a reference by Nanoview) as the top layer, SiO₂ (described by a Cauchy model) as the interfacial native oxide layer, and Si (measured and modeled as a reference by Nanoview) as the substrate. The amount of Ge atoms was evaluated based on layer density measured by X-ray fluorescence (XRF, ARL QUANT'X, Thermo Scientific). The quantity of Ge was calibrated using standard samples that had been verified through Rutherford backscattering spectroscopy (RBS). The crystallographic structures of GeO₂ were investigated using GAXRD (SmartLab, Rigaku), the measurements were carried out with the Cu K_α emission line, the angular range was 10–80° in 2θ, and the step size was 0.01° in 2θ. The impurity concentration in the films was examined through AES (PHI 700, Physical Electronics) with the electron beam energies of 10 keV with the beam at an angle of 60° to the surface normal. Argon ions (Ar⁺) were accelerated to 1 kV and used to etch the thin film at a rate of 0.2 min/step in order to acquire an in-depth profile. The chemical binding states of the deposited films were investigated by using XPS (K-Alpha, Thermo Scientific) equipped with a monochromatic Al K_α X-ray source. A pass energy of 200.0 eV was utilized, and the peak shift was correctly corrected with respect to the C 1s peak. In order to eliminate surface contamination, a 10 s 2 kV Ar⁺ sputtering process was conducted.

Crystallography. Single crystals of complexes 1 and 7 were grown from their saturated solutions in hexane at room temperature. In a typical procedure, a specimen of suitable size and quality was obtained from the solution, coated with Paratone oil, and mounted on a glass capillary. Reflection data were collected using a Bruker SMART APEX II-CCD area detector diffractometer with graphite-monochromated Mo K_α radiation ($\lambda = 0.71073$ Å). The hemisphere of the reflection data was collected as ω -scan frames with 0.3° per frame and an exposure time of 10 s per frame. Cell parameters were determined and refined using the SMART program.⁶⁸ Data reduction was performed using SAINT software.⁶⁹ The data were corrected for Lorentz and polarization effects, and an empirical absorption correction was applied using the SADABS program.⁷⁰ The structures of the prepared compounds were solved by direct methods and all non-hydrogen atoms were subjected to anisotropic refinement by the full-matrix least-squares method on F^2 using the SHELXTL/PC package.⁷¹ Hydrogen atoms were placed at their geometrically calculated positions and refined based on the corresponding carbon

atoms with isotropic thermal parameters. CCDC 2257110–2257111 for complexes 1 and 7 contain the supplementary crystallographic data for this article.

CONCLUSIONS

Herein, we described the synthesis, structure, and characterization of germanium complexes 1–12 stabilized by β -diketonate and/or *N*-alkoxy functionalized carboxamidate ligands as potential candidates for GeO₂ ALD. In this series, complexes 1 and 2 contained β -diketonate ligands and chlorine, whereas complexes 3–12 were heteroleptic compounds comprising one β -diketonate ligand and one carboxamidate ligand. Complexes 1 and 7 crystallized as monomers, and the coordination geometry of 1 can be described as a distorted trigonal pyramidal structure in the solid state. Compound 7 also exhibited a 4-coordinated core atom with a distorted seesaw molecular geometry. The thermal stabilities and volatilities of complexes 1–12 were evaluated by TGA. All of the complexes exhibited single-step evaporation in their TGA curves. Complexes 3–7 exhibited high residues of up to 47.1% with poor vaporization; however, compound 1 exhibited a residual of 3.4%. In contrast, 2 and 8–12 containing tmhd exhibited higher volatility with weight losses of 98% (11), particularly complex 2 with no residue, which started thermal volatilization at 103 °C and was completed at 197.8 °C. Therefore, liquid compound 2 exhibited useful properties for application as an ALD precursor. GeO₂ thin films were subsequently grown by ALD using 2 as a new precursor and H₂O₂ as the reactant at deposition temperatures ranging from 300 to 350 °C. Self-limiting film growth with a saturated GPC of approximately 0.27 Å/cycle at 300 °C was observed based on both precursor and reactant pulsing times. Saturation behavior without an incubation cycle was observed, and a stoichiometric GeO₂ film with a low impurity level was formed, owing to the robust ALD characteristics of this precursor.

ASSOCIATED CONTENT

Supporting Information

The Supporting Information is available free of charge at <https://pubs.acs.org/doi/10.1021/acsomega.3c05657>.

NMR, FT-IR spectra of complexes 1–12, and data collection parameters for complexes 1 and 7 (PDF)

Crystallographic data for complex 1 (CIF)

Crystallographic data for complex 7 (CIF)

AUTHOR INFORMATION

Corresponding Authors

Taeyong Eom – Thin Film Materials Research Center, Korea Research Institute of Chemical Technology (KRICT), Daejeon 34114, Republic of Korea; orcid.org/0000-0002-9646-9553; Email: eomt@kRICT.re.kr

Taek-Mo Chung – Thin Film Materials Research Center, Korea Research Institute of Chemical Technology (KRICT), Daejeon 34114, Republic of Korea; Department of Chemical Convergence Materials, University of Science and Technology (UST), Daejeon 34113, Republic of Korea; orcid.org/0000-0002-5169-2671; Email: tmchung@kRICT.re.kr

Authors

Heenang Choi – Thin Film Materials Research Center, Korea Research Institute of Chemical Technology (KRICT),

Daejeon 34114, Republic of Korea; Department of Chemistry, Sungkyunkwan University (SKKU), Suwon-si, Gyeonggi-do 16419, Republic of Korea

Chanwoo Park – Thin Film Materials Research Center, Korea Research Institute of Chemical Technology (KRICT), Daejeon 34114, Republic of Korea

Sung Kwang Lee – Thin Film Materials Research Center, Korea Research Institute of Chemical Technology (KRICT), Daejeon 34114, Republic of Korea

Ji Yeon Ryu – Thin Film Materials Research Center, Korea Research Institute of Chemical Technology (KRICT), Daejeon 34114, Republic of Korea; orcid.org/0000-0001-6321-5576

Seung Uk Son – Department of Chemistry, Sungkyunkwan University (SKKU), Suwon-si, Gyeonggi-do 16419, Republic of Korea; orcid.org/0000-0002-4779-9302

Complete contact information is available at:

<https://pubs.acs.org/10.1021/acsomega.3c05657>

Author Contributions

The manuscript was written through contributions of all authors. All authors have given approval to the final version of the manuscript.

Notes

The authors declare no competing financial interest.

ACKNOWLEDGMENTS

We are grateful to Hongseok Jang of Oceanbridge Co., Ltd. R&D Center for helping with the TG analysis. This work was supported by the Development of Smart Chemical Materials for IoT Devices Project through the Korea Research Institute of Chemical Technology (KRICT) of Republic of Korea (KS2321-10) and the National R&D Program through a National Research Foundation of Korea (NRF) grant funded by the Ministry of Science and ICT (2021M3D1A2045614).

ABBREVIATIONS

AES, Auger electron spectroscopy; ALD, atomic layer deposition; CVD, chemical vapor deposition; EA, elemental analysis; FT-IR, Fourier transform infrared; GAXRD, glancing angle X-ray diffraction; GPC, growth per cycle; MS, mass spectrometry; NMR, nuclear magnetic resonance; TGA, thermogravimetric analysis; XPS, X-ray photoelectron spectroscopy

REFERENCES

- (1) Koziej, D.; Bãrsan, N.; Shimano, K.; Yamazoe, N.; Szuber, J.; Weimar, U. Spectroscopic insights into CO sensing of undoped and palladium doped tin dioxide sensors derived from hydrothermally treated tin oxide sol. *Sens. Actuators, B* **2006**, *118*, 98–104.
- (2) Manjunathan, P.; Marakatti, V. S.; Chandra, P.; Kulal, A. B.; Umbarkar, S. B.; Ravishankar, R.; Shanbhag, G. V.; et al. Mesoporous tin oxide: an efficient catalyst with versatile applications in acid and oxidation catalysis. *Catal. Today* **2018**, *309*, 61–76.
- (3) Yang, J.; Cheng, F.; Zhu, Z.; Feng, J.; Xue, M.; Meng, Z.; Qiu, L. An enhanced gas sensor based on SiO₂@mesoporous MCM-41 core-shell nanocomposites for SO₂ visual detection. *Analyst* **2020**, *145*, 4352–4357.
- (4) Seo, T.; Park, H.; Jeon, G.; Yun, J.; Park, S.; Seong, S.; Chung, Y. Low-Temperature Fabrication (≤ 150 °C) of High-Quality Sputtered Silicon Oxide Thin Film with Hydrogen Plasma Treatment. *ACS Appl. Electron. Mater.* **2020**, *2*, 3320–3326.
- (5) Hu, C.; McDaniel, M. D.; Jiang, A.; Posadas, A.; Demkov, A. A.; Ekerdt, J. G.; Yu, E. T. A Low-Leakage Epitaxial High- κ Gate Oxide

for Germanium Metal-Oxide-Semiconductor Devices. *ACS Appl. Mater. Interfaces* **2016**, *8*, 5416–5423.

(6) Cruz, A.; Erfurt, D.; Wagner, P.; Morales-Vilches, A. B.; Ruske, F.; Schlattmann, R.; Stannowski, B. Optoelectrical analysis of TCO +Silicon oxide double layers at the front and rear side of silicon heterojunction solar cells. *Sol. Energy Mater. Sol. Cells* **2022**, *236*, 111493.

(7) Esro, M.; Georgakopoulos, S.; Lu, H.; Vourlias, G.; Krier, A.; Milne, W. I.; Gillin, W. P.; Adamopoulos, G. Solution processed SnO₂:Sb transparent conductive oxide as an alternative to indium tin oxide for applications in organic light emitting diodes. *J. Mater. Chem. C* **2016**, *4*, 3563–3570.

(8) Yoon, C. M.; Oh, I.-K.; Lee, Y.; Song, J.-G.; Lee, S. J.; Myoung, J.-M.; Kim, H. G.; Moon, H.-S.; Shong, B.; Lee, H.-B.-R.; Kim, H. Water-Erasable Memory Device for Security Applications Prepared by the Atomic Layer Deposition of GeO₂. *Chem. Mater.* **2018**, *30*, 830–840.

(9) Delabie, A.; Bellenger, F.; Houssa, M.; Conard, T.; Van Elshocht, S.; Caymax, M.; Heyns, M.; Meuris, M. Effective electrical passivation of Ge(100) for high- κ gate dielectric layers using germanium oxide. *Appl. Phys. Lett.* **2007**, *91*, 082904.

(10) Novotny, L.; Hecht, B. *Principles of Nano-Optics*; Cambridge University Press, 2007.

(11) Prasad, P. N. *Nanophotonics*; Wiley: New York, 2004.

(12) Kar, S. *High Permittivity Gate Dielectric Materials*; Springer, 2013.

(13) Perego, M.; Scarel, G.; Fanciulli, M.; Fedushkin, I. L.; Skatova, A. A. Fabrication of GeO₂ layers using a divalent Ge precursor. *Appl. Phys. Lett.* **2007**, *90*, 162115.

(14) Takahashi, H.; Sugimoto, I. A germanium-oxide glass optical fiber prepared by a VAD method. *J. Lightwave Technol.* **1984**, *2*, 613–616.

(15) Matsuura, Y. Optical fibers for medical applications. *Lasers Med. Sci.* **2013**, *110*–124.

(16) Hermet, P.; Fraysse, G.; Lignie, A.; Armand, P.; Papet, P. Density Functional Theory Predictions of the Nonlinear Optical Properties in α -Quartz-type Germanium Dioxide. *J. Phys. Chem. C* **2012**, *116*, 8692–8698.

(17) Lignie, A.; Armand, P.; Papet, P. Growth of Piezoelectric Water-Free GeO₂ and SiO₂-Substituted GeO₂ Single-Crystals. *Inorg. Chem.* **2011**, *50*, 9311–9317.

(18) Yankov, G.; Dimowa, L.; Petrova, N.; Tarassov, M.; Dimitrov, K.; Petrov, T.; Shivachev, B. L. Synthesis, structural and non-linear optical properties of TeO₂-GeO₂-Li₂O glasses. *Opt. Mater.* **2012**, *35*, 248–251.

(19) Shang, M.; Chen, X.; Li, B.; Niu, J. A Fast Charge/Discharge and Low-Temperature Battery with Germanium Oxide Layer on Ti₃C₂ MXene Matrix as Anode. *ACS Nano* **2020**, *14*, 3678–3686.

(20) Qasrawi, A. F.; Daragme, R. Design and Characterization of (Yb, Al, Cu, Au)/GeO₂/C As MOS Field Effect Transistors, Negative Capacitance Effect Devices and Band Pass/Reject Filters Suitable for 4G Technologies. *J. Electron. Mater.* **2022**, *51*, 2510–2520.

(21) Arro, C. R.; Mohamed, A. T. I.; Bensalah, N. Impact of Ge content on the electrochemical performance of Germanium Oxide/Germanium/ reduced graphene (GeO₂/Ge/r-GO) hybrid composite anodes for lithium-ion batteries. *Mater. Today Commun.* **2022**, *30*, 103151.

(22) Huo, K.; Wang, L.; Peng, C.; Peng, X.; Li, Y.; Li, Q.; Jin, Z.; Chu, P. K. Crumpled N-doped carbon nanotubes encapsulated with peapod-like Ge nanoparticles for high-rate and long-life Li-ion battery anodes. *J. Mater. Chem.* **2016**, *4*, 7585–7590.

(23) Farbod, B.; Cui, K.; Kalisvaart, W. P.; Kupsta, M.; Zahiri, B.; Kohandehghan, A.; Lotfabad, E. M.; Li, Z.; Luber, E. J.; Mitlin, D. Anodes for Sodium Ion Batteries Based on Tin-Germanium-Antimony Alloys. *ACS Nano* **2014**, *8*, 4415–4429.

(24) Baggetto, L.; Keum, J. K.; Browning, J. F.; Veith, G. M. Germanium as negative electrode material for sodium-ion batteries. *Electrochem. Commun.* **2013**, *34*, 41–44.

- (25) Abel, P. R.; Lin, Y.-M.; de Souza, T.; Chou, C.-Y.; Gupta, A.; Goodenough, J. B.; Hwang, G. S.; Heller, A.; Mullins, C. B. Nanocolumnar Germanium Thin Films as a High-Rate Sodium-Ion Battery Anode Material. *J. Phys. Chem. C* **2013**, *117*, 18885–18890.
- (26) Feng, J.; Hu, W.; Zeng, F.; Lin, H.; Li, L.; Yang, B.; Peng, Y.; Wu, D.; Huo, B.; Tang, X. Investigation of physically transient resistive switching memory based on GeO₂ thin films. *Appl. Phys. Lett.* **2020**, *117*, 192102.
- (27) Seal, M.; Bose, N.; Mukherjee, S. Application of GeO₂ nanoparticle as electrically erasable memory and its photo catalytic behaviour. *Mater. Res. Express* **2018**, *5*, 065007.
- (28) Chang, T. C.; Yan, S. T.; Hsu, C. H.; Tang, M. T.; Lee, J. F.; Tai, Y. H.; Liu, P. T.; Sze, S. M. A distributed charge storage with GeO₂ nanodots. *Appl. Phys. Lett.* **2004**, *84*, 2581–2583.
- (29) Walker, B.; Dharmawardhana, C. C.; Dari, N.; Rulis, P.; Ching, W.-Y. Electronic structure and optical properties of amorphous GeO₂ in comparison to amorphous SiO₂. *J. Non-Cryst. Solids* **2015**, *428*, 176–183.
- (30) Micoulaut, M.; Cormier, L.; Henderson, G. S. The structure of amorphous, crystalline and liquid GeO₂. *J. Phys.: Condens. Matter* **2006**, *18*, R753–R784.
- (31) Berghuis, W. J. H.; Melskens, J.; Macco, B.; Theeuwes, R. J.; Verheijen, M. A.; Kessels, W. M. M. Surface passivation of germanium by atomic layer deposited Al₂O₃ nanolayers. *J. Mater. Res.* **2021**, *36*, 571–581.
- (32) Beer, C. Fabrication and Characterisation of Novel Ge MOSFETs. Ph.D. Thesis, University of Warwick, 2007.
- (33) Antoja-Lleonart, J.; Zhou, S.; de Hond, K.; Huang, S.; Koster, G.; Rijnders, G.; Noheda, B. Atomic layer deposition of SiO₂-GeO₂ multilayers. *Appl. Phys. Lett.* **2020**, *117*, 041601.
- (34) Goley, P. S.; Hudait, M. K. Germanium Based Field-Effect Transistors: Challenges and Opportunities. *Materials* **2014**, *7*, 2301–2339.
- (35) Pillarisetty, R. Academic and industry research progress in germanium nanodevices. *Nature* **2011**, *479*, 324–328.
- (36) Johnson, O. H. Germanium and its Inorganic Compounds. *Chem. Rev.* **1952**, *51*, 431–469.
- (37) Almuslem, A. S.; Hanna, A. N.; Yapici, T.; Wehbe, N.; Diallo, E. M.; Kutbee, A. T.; Bahabry, R. R.; Hussain, M. M. Water soluble nano-scale transient material germanium oxide for zero toxic waste based environmentally benign nano-manufacturing. *Appl. Phys. Lett.* **2017**, *110*, 074103.
- (38) Lange, T.; Njoroge, W.; Weis, H.; Beckers, M.; Wuttig, M. Physical properties of thin GeO₂ films produced by reactive DC magnetron sputtering. *Thin Solid Films* **2000**, *365*, 82–89.
- (39) Kita, K.; Suzuki, S.; Nomura, H.; Takahashi, T.; Nishimura, T.; Toriumi, A. Direct Evidence of GeO Volatilization from GeO₂/Ge and Impact of Its Suppression on GeO₂/Ge Metal-Insulator-Semiconductor Characteristics. *Jpn. J. Appl. Phys.* **2008**, *47*, 2349–2353.
- (40) Pantelides, S. T.; Harrison, W. A. Electronic structure, spectra, and properties of 4:2-coordinated materials. I. Crystalline and amorphous SiO₂ and GeO₂. *Phys. Rev. B* **1976**, *13*, 2667–2691.
- (41) Lucat, C.; Ginet, P.; Castille, C.; Debéda, H.; Ménil, F. Microsystems elements based on free-standing thick-films made with a new sacrificial layer process. *Microelectron. Reliab.* **2008**, *48*, 872–875.
- (42) Sangrador, J.; Olivares, J.; Iborra, E.; Vergara, L.; Clement, M.; Sanz-Hervas, A. Ge and GeO_x films as sacrificial layer for MEMS technology based on piezoelectric AlN: etching and planarization processes. *Smart Sensors, Actuators, and MEMS II*, 2005; Vol. 5836, pp 1–15.
- (43) Lorenz, H.; Zhao, Q.; Turner, S.; Lebedev, O. I.; Van Tendeloo, G.; Klötzer, B.; Rameshan, C.; Penner, S. Preparation and structural characterization of SnO₂ and GeO₂ methanol steam reforming thin film model catalysts by (HR)TEM. *Mater. Chem. Phys.* **2010**, *122*, 623–629.
- (44) Khan, M. A.; Hogan, T. P.; Shanker, B. Surface-enhanced Raman scattering from gold-coated germanium oxide nanowires. *J. Raman Spectrosc.* **2008**, *39*, 893–900.
- (45) Okumura, K.; Asakura, K.; Iwasawa, Y. Characterization of GeO₂ Sub-monolayers on SiO₂ Prepared by Chemical Vapor Deposition of Ge(OMe)₄ by EXAFS, FT-IR, and XRD. *Langmuir* **1998**, *14*, 3607–3613.
- (46) Triyoso, D.; Liu, R.; Roan, D.; Ramon, M.; Edwards, N. V.; Gregory, R.; Werho, D.; Kulik, J.; Tam, G.; Irwin, E.; Wang, X.-D., Jr.; La, L. B.; Hobbs, C.; Garcia, R.; Baker, J.; White, B. E.; Tobin, P. Impact of Deposition and Annealing Temperature on Material and Electrical Characteristics of ALD HfO₂. *J. Electrochem. Soc.* **2004**, *151*, F220.
- (47) Johnson, R. W.; Hultqvist, A.; Bent, S. F. A brief review of atomic layer deposition: from fundamentals to applications. *Mater. Today* **2014**, *17*, 236–246.
- (48) Oviroh, P. O.; Akbarzadeh, R.; Pan, D.; Coetzee, R. A. M.; Jen, T.-C. New development of atomic layer deposition: processes, methods and applications. *Sci. Technol. Adv. Mater.* **2019**, *20*, 465–496.
- (49) Schilirò, E.; Lo Nigro, R.; Roccaforte, F.; Giannazzo, F. Substrate-Driven Atomic Layer Deposition of High-κ Dielectrics on 2D Materials. *Appl. Sci.* **2021**, *11*, 11052.
- (50) Nam, T.; Kim, H. Atomic layer deposition for nonconventional nanomaterials and their applications. *J. Mater. Res.* **2019**, *35*, 656–680.
- (51) Kim, K. H.; Gordon, R. G.; Ritenour, A.; Antoniadis, D. A. Atomic layer deposition of insulating nitride interfacial layers for germanium metal oxide semiconductor field effect transistors with high-κ oxide/tungsten nitride gate stacks. *Appl. Phys. Lett.* **2007**, *90*, 212104.
- (52) Jung, J.-S.; Kim, D.-H.; Shin, J.-H.; Kang, J.-G. Atomic Layer Deposition of GeO₂ Thin Films on Si(100) using Ge(N,N'-R,R-en)(NMe₂)₂ (Where R = Isopropyl and *t*-Butyl) Precursors. *Bull. Korean Chem. Soc.* **2015**, *36*, 1953–1954.
- (53) George, S. M.; Park, B. K.; Kim, C. G.; Chung, T.-M. Heteroleptic Group 2 Metal Precursors for Metal Oxide Thin Films. *Eur. J. Inorg. Chem.* **2014**, 2002–2010.
- (54) Database of ALD processes, DOI: 10.6100/alddbatabase. <http://www.atomiclimits.com/alddbatabase/> (accessed Jul 25, 2023).
- (55) George, S. M.; Nam, J. H.; Lee, G. Y.; Han, J. H.; Park, B. K.; Kim, C. G.; Jeon, D. J.; Chung, T.-M. *N*-Alkoxy Carboxamide Stabilized Tin(II) and Germanium(II) Complexes for Thin-Film Applications. *Eur. J. Inorg. Chem.* **2016**, 5539–5546.
- (56) Schwarberg, J. E.; Sievers, R. E.; Moshier, R. W. Gas chromatographic and related properties of the alkaline earth chelates with 2,2,6,6-tetramethyl-3,5-heptanedione. *Anal. Chem.* **1970**, *42*, 1828–1830.
- (57) Hatanpää, T.; Ritala, M.; Leskelä, M. Precursors as enablers of ALD technology: Contributions from University of Helsinki. *Coord. Chem. Rev.* **2013**, *257*, 3297–3322.
- (58) Dunbar, A. C.; Joseph Lastowski, R.; Girolami, G. S. Synthesis and Characterization of Strontium *N,N*-Dimethylaminodiboranates as Possible Chemical Vapor Deposition Precursors. *Inorg. Chem.* **2020**, *59*, 16893–16904.
- (59) Rodgers, A.; Stobart, S. R. Monomeric derivatives of bivalent germanium: keto-enolate and related chelate compounds. *J. Chem. Soc., Chem. Commun.* **1976**, 52–53.
- (60) Pacansky, J.; Koch, W.; Miller, M. D. Analysis of the structures, infrared spectra, and Raman spectra for methyl, ethyl, isopropyl, and *tert*-butyl radicals. *J. Am. Chem. Soc.* **1991**, *113*, 317–328.
- (61) Garg, P.; Dange, D.; Jones, C. *s*- and *p*-Block Dinuclear Metal(Ioid) Complexes Bearing 1,4-Phenylene and 1,4-Cyclohexylene Bridged Bis(amidinate) Ligands. *Eur. J. Inorg. Chem.* **2020**, 4037–4044.
- (62) Klüfers, P.; Vogler, C. Polyol Metal Complexes. Part 55 Germanes with Alkylendioxy Substituents. *Z. Anorg. Allg. Chem.* **2007**, *633*, 908–912.

(63) Airapetyan, D. V.; Murasheva, T. P.; Bylikin, S. Y.; Korlyukov, A. A.; Shipov, A. G.; Gruener, S. V.; Kramarova, E. P.; Negrebetskii, V. V.; Pogozhikh, S. A.; Zueva, G. Y.; Antipin, M. Y.; Baukov, Y. I. Trichloro- and methylchlorogermyl monochelates and dibromo- and dichlorogermyl bischelates derived from *N,N*-disubstituted amides of 2-hydroxycarboxylic acids. *Russ. Chem. Bull.* **2012**, *61*, 642–651.

(64) As determined from a survey of the Cambridge Crystallographic Database, January, 2008.

(65) Schmeisser, D.; Schnell, R. D.; Bogen, A.; Himpfel, F. J.; Rieger, D.; Landgren, G.; Morar, J. F. Surface oxidation states of germanium. *Surf. Sci.* **1986**, *172*, 455–465.

(66) Crist, B. V. *Handbook of Monochromatic XPS Spectra*; Wiley, 1999; Vol. 2.

(67) Gottlieb, H. E.; Kotlyar, V.; Nudelman, A. NMR Chemical Shifts of Common Laboratory Solvents as Trace Impurities. *J. Org. Chem.* **1997**, *62*, 7512–7515.

(68) SMART. version 5.0, Data collection software; Bruker AXS, Inc.: Madison, WI, 1998;.

(69) SAINT. version 5.0, Data integration software; Bruker AXS, Inc.: Madison, WI, 1998;.

(70) Sheldrick, G. M. *SADABS, Program for Absorption correction with the Bruker SMART system*; Universitat Göttingen: Germany, 1996.

(71) Sheldrick, G. M. *SHELXL-93: Program for the refinement of crystal structures*; Universitat Göttingen: Germany, 1993.